



Article

Development of ZnFeCe Layered Double Hydroxide Incorporated Thin Film Nanocomposite Membrane with Enhanced Separation Performance and Antibacterial Properties

Cigdem Balcik ^{1,*}, Bahar Ozbey-Unal ^{1,2}, Busra Sahin ³, Ecem Buse Aydın ¹, Bengisu Cifcioglu-Gozuacik ¹, Ramazan Keyikoglu ^{1,4}  and Alireza Khataee ^{1,5,*} 

¹ Department of Environmental Engineering, Gebze Technical University, 41400 Gebze, Turkey

² Institute of Earth and Marine Sciences, Gebze Technical University, 41400 Gebze, Turkey

³ Department of Biotechnology, Gebze Technical University, 41400 Gebze, Turkey

⁴ Department of Environmental Engineering, Faculty of Engineering and Natural Sciences, Bursa Technical University, 16310 Bursa, Turkey

⁵ Research Laboratory of Advanced Water and Wastewater Treatment Processes, Department of Applied Chemistry, Faculty of Chemistry, University of Tabriz, Tabriz 51666-16471, Iran

* Correspondence: cigdembalcik@gtu.edu.tr (C.B.); akhataee@gtu.edu.tr (A.K.)

Abstract: Developing thin-film nanocomposite (TFN) membranes by incorporating nanomaterials into the selective polyamide (PA) layer is an effective strategy to improve separation and antibacterial properties. In this study, TFN nanofiltration (NF) membranes were fabricated by interfacial polymerization of piperazine (PIP) and trimesoyl chloride (TMC) with the addition of Zinc-Iron-Cerium (ZnFeCe) layered double hydroxide (LDH). The improved surface hydrophilicity of TFN membranes was investigated by water contact angle analyses and pure water flux measurements. Successful production of the PA layer on the membrane surface was determined by Fourier-transform infrared (FTIR) analysis. Atomic Force Microscope (AFM) images showed that the addition of LDH into the membrane resulted in a smoother surface. The scanning electron microscope and energy-dispersive X-ray spectroscopy (SEM/EDS) mapping of TFN membrane proved the presence of Ce, Fe, and Zn elements, indicating the successful addition of LDH nanoparticles on the membrane surface. TFN 3 membrane was characterized with the highest flux resulting in 161% flux enhancement compared to the pristine thin film composite (TFC) membrane. All membranes showed great rejection performances (with a rejection higher than 95% and 88% for Na₂SO₄ and MgSO₄, respectively) for divalent ions. Additionally, TFN membranes exhibited excellent antibacterial and self-cleaning properties compared to the pristine TFC membrane.

Keywords: thin film membrane; layered double hydroxide; nanofiltration; salt removal



Citation: Balcik, C.; Ozbey-Unal, B.; Sahin, B.; Buse Aydın, E.; Cifcioglu-Gozuacik, B.; Keyikoglu, R.; Khataee, A. Development of ZnFeCe Layered Double Hydroxide Incorporated Thin Film Nanocomposite Membrane with Enhanced Separation Performance and Antibacterial Properties. *Water* **2023**, *15*, 264. <https://doi.org/10.3390/w15020264>

Academic Editor: Peyman Gholami

Received: 1 December 2022

Revised: 3 January 2023

Accepted: 4 January 2023

Published: 8 January 2023



Copyright: © 2023 by the authors. Licensee MDPI, Basel, Switzerland. This article is an open access article distributed under the terms and conditions of the Creative Commons Attribution (CC BY) license (<https://creativecommons.org/licenses/by/4.0/>).

1. Introduction

Water scarcity is a critical issue that is mainly caused by an increase in world population, industrialization, climate change, and improper management of water resources [1]. Water reuse and desalination processes are feasible and efficient solutions for freshwater production. The development of practical, affordable, and environmentally friendly membrane processes is the focus of seawater desalination, wastewater treatment, and wastewater recovery/reuse studies [2]. Thin film composite (TFC) membranes are widely known as the most efficient membrane technology for desalination. Unfortunately, they face some important drawbacks such as low water permeability, low salt rejection, low chlorine tolerance, fouling, etc. Many attempts have been made to enhance the separation performances of TFC membranes. These efforts resulted in the fabrication of nanomaterial-incorporated TFC membranes that are also known as thin film nanocomposite (TFN) membranes [3].

Previous studies proved that the composition and structure of nanomaterials affect the characteristics of TFN membranes [4–6]. The use of TFN membranes can enhance water flux without a compromise in the salt rejection ratio compared with the pristine TFC membranes [7,8]. In recent years, more research has concentrated on the fabrication of TFN membranes using various types of nanomaterials i.e., carbon nanotubes [9], metal-organic frameworks (MOFs) [10], graphene/graphene oxide [11], titanium dioxide [12], clays [13] and layer double hydroxides (LDHs) [14].

LDHs have gained popularity in a variety of fields, including energy, water treatment, biomedical, electrochemistry, and photochemistry because of their highly customizable structures [15]. LDHs, as nanofillers, can improve water attraction properties of membranes creating extra diffusion channels due to their inherent hydrophilicity. In addition, their unique layered structure with distinct interlayer spacing can act as a molecular sieving mechanism by providing an extra water transport pathway [16]. CoNi LDH incorporated loose NF membrane achieved a methylene blue rejection rate of 97.9% and a water permeability of $198.6 \text{ L}/(\text{m}^2\text{hMPa})$ [17]. In another study, CoAl LDH improved the hydrophilicity of the reverse osmosis membrane, which achieved a $55 \text{ Lm}^{-2}\text{h}^{-1}$ greater water permeability and a salt rejection of 99.03% [18]. Moreover, the TFN membrane coupled with ZnAl LDH achieved higher Cd^{+2} and Pb^{+2} rejection rates than that of the pristine membrane [19].

The growth of bacteria on the membrane, which is called biofouling, is a greater issue compared to other fouling types in NF applications. In this regard, cerium-containing nanoparticles act as effective antibacterial agents against pathogens with their unique state of Ce(III) and Ce(IV) [20]. Furthermore, the addition of ions with 4f electronic configurations as a dopant in semiconductor materials enhances photocatalytic activity [21]. Especially, Ce 4f levels affect the photo-induced charge formation and transfer. Therefore, the special electronic structure of Ce enhances the optical and photocatalytic properties of the hosting material. For instance, Ce^{4+} can decrease electron-hole recombination by acting as a trap for photogenerated electrons [22]. Similarly, Zn is a suitable candidate in the hydroxide layers of LDHs owing to its high photocatalytic efficiency, chemical durability, and low toxicity [23].

As stated in previous studies, membrane fouling, which is the biggest obstacle to the use of pressure-driven membranes, can be mitigated the incorporating hydrophilic nanoparticles. Although LDHs have potential as nanofillers, their use in membrane fabrication has been rarely investigated. In this study, TFN membranes using ZnFeCe LDH with different loadings were produced by the conventional interfacial polymerization (IP) technique. The effect of ZnFeCe LDH on the membrane hydrophilicity, morphology, and porosity was investigated. The optimum amount of ZnFeCe LDH in the TFN membrane was determined based on the filtration and antifouling performances of the membranes. Finally, the antibacterial properties of the TFN membrane were investigated using bacterial viability inhibition tests

2. Materials and Methods

2.1. Materials

Polyethersulfone (PES) ultrafiltration (UF) membrane with a 20 kDa molecular weight cut-off (UP020, Microdyn Nadir, Germany) was used as a support membrane. n-hexane was obtained from Merck Co (Germany). 3,5-benzene-tricarbonyl trichloride (TMC, 99% purity), piperazine (PIP, 99% purity), Iron(III) chloride hexahydrate ($\text{FeCl}_3\cdot 6\text{H}_2\text{O}$), Zinc chloride (ZnCl_2 , 99%), Cerium(III) nitrate hexahydrate ($\text{Ce}(\text{NO}_3)_3\cdot 6\text{H}_2\text{O}$), sodium hydroxide pellets (NaOH, 99%), sodium chloride (NaCl), magnesium chloride (MgCl_2), sodium sulfate (Na_2SO_4) and magnesium sulfate (MgSO_4) were supplied from Sigma-Aldrich (Germany). Reactive red 198 (Mw: 984.21 g/mol) was supplied for DyStar (Singapore).

2.2. Synthesis of ZnFeCe LDH

ZnFeCe LDH with an $\text{M}^{2+}/\text{M}^{3+}$ molar ratio of 3 was prepared using the co-precipitation technique [24]. 3 mM ZnCl_2 , 0.5 mM $\text{FeCl}_3\cdot 6\text{H}_2\text{O}$, and 0.5 mM $\text{Ce}(\text{NO}_3)_3\cdot 6\text{H}_2\text{O}$ were added

in pure water purged under N₂ atmosphere. The prepared solution was maintained at pH 8 by the gentle addition of NaOH while vigorously mixing. Then the solution was subjected to a 24-h aging period. The samples were centrifuged, and the catalyst was separated from the solution. The resulting solid was washed several times using ethanol and water. Then, it was dried by heating it in the oven at 50 °C for 7 h yielded. The ZnFeCe LDH was obtained by grinding and sieving the solid powder.

2.3. Characterization of ZnFeCe LDH

The crystalline structure of the ZnFeCe LDH was determined by an X-ray diffraction analyzer (Rigaku Rint 2200, Japan) Fourier-transform infrared (FTIR) analysis was carried out for determining functional groups, and the interactions between layers of the ZnFeCe LDH (Perkin Elmer Spectrum 100, Germany). The membrane surface property and elemental composition were investigated by a scanning electron microscope (Philips XL30 SFEG, The Netherlands) and energy-dispersive X-ray spectroscopy (EDS) analyses. A high-resolution transmission electron microscope (TEM) operated at 200 kV (HRTEM: Japan JEOL JEM-2100 Plus, Japan) was utilized to take TEM images. Brunauer-Emmett-Teller (BET) method was used to calculate the pore diameter, pore volume of the sample, and specific surface area by the BELSORP model of Mini II (Japan).

2.4. Fabrication of Membranes

PES UF membrane was used as the support in the production of TFC membrane by conventional IP technique. PIP and TMC/n-hexane solutions were employed as organic and inorganic solvents, respectively. In a typical procedure, the UF substrate membrane was placed in the module. 20 mL of 1 wt.% of PIP solution was poured over the UF membrane and waited for five minutes. The excess solution was poured out and the membrane was removed from the module and left to dry. Then, it was placed back in the module and 20 mL TMC/n-hexane solution (% 0.1 (*w/v*)) was added. After one min contact time, the excess solution was taken off and the surface of the membrane was washed out with n-hexane to cease the reaction of PIP and TMC/n-hexane. Finally, the fabricated membranes were post-treated in an oven at 60 °C for 5 min. Produced membranes were immersed in pure water until they were used. For the fabrication of TFN membranes, a certain amount of LDH was added to the TMC/n-hexane solution. The fabricated TFC membranes containing different amounts of LDHs in the polyamide (PA) layers were named TFN 1, TFN 2, TFN 3, and TFN 4 (Table 1). A pristine TFC control membrane without the addition of LDH was referred to as TFC.

Table 1. The composition of the produced membranes.

Membrane	PIP (wt.%)	TMC/n-Hexane (wt./v%)	LDH Content in TMC Solution (wt./v%)
TFC	1	0.10	0
TFN 1	1	0.10	0.01
TFN 2	1	0.10	0.05
TFN 3	1	0.10	0.10
TFN 4	1	0.10	0.20

2.5. Membrane Characterization

To investigate the membrane hydrophilicity, contact angle measurements were performed by a goniometer (KSV Instruments, CAM101, Finland). The structural and functional groups on the membrane surface were determined by Fourier-transform infrared spectroscopy (FTIR) (Perkin Elmer, USA). A scanning electron microscope (SEM) coupled with an SEM/Energy-dispersive X-ray spectroscopy (EDS) was used to identify the membrane surface characteristics and elemental composition (Tescan Mira3, Czech Republic). Atomic Force Microscope (AFM) was used to determine the membrane surface roughness (Digital Instruments Nanoscope, India).

2.6. Separation

A filtration system with a membrane area of 14.6 cm² was used for the filtration studies. The transmembrane pressure was maintained at 10 bars. Firstly, the membranes were compacted at 11 bars for 60 min to reach a steady-state permeate flux. The permeate flux was calculated according to Equation (1):

$$J_w = \frac{m}{A \cdot t} \quad (1)$$

where J_w refers to the pure water flux (PWF), m is the permeate mass, A is the membrane area, and t is the time.

Desalination performances of the fabricated membrane were evaluated with filtration of Na₂SO₄, MgSO₄, MgCl₂, and NaCl solutions (2 g/L) at 10 bars. Dye/salt separation performances were determined with filtration of 3 different solutions (100 mg/L dye, 2 g/L NaCl, and 100 mg/L dye+2 g/L NaCl solution). The concentrations of dye were analyzed spectrophotometrically by a spectrophotometer (Hach Lange DR 6000, USA) and NaCl separation efficiency was measured as changes in conductivity using a multiparameter. All tests were performed in triplicates for each membrane.

2.7. Photodegradation Studies

The photodegradation properties of fabricated membranes were determined by applying an AAA-class solar simulator coupled with a 100W Xenon lamp (Fytronix, Turkey). The membranes (TFC and TFN 3) were subjected to a dye solution with a concentration of 200 mg/L for 24 h. After that, the membranes were rinsed with distilled to remove the attached dyes on the membrane surface. Then, membranes were exposed to visible light for 15 min to observe the visual changes on the membrane surface caused by photocatalytic degradation. The photograph of membranes was taken before and after photodegradation studies to determine the effect of the photodegradation process.

2.8. Antibacterial Properties

Antibacterial characteristics of the fabricated membranes were determined by bacterial viability inhibition tests using *Escherichia coli* BL21 (Amersham Biosciences, Buckinghamshire, UK). Cell viability of ZnFeCe LDH nanomaterial against *E. coli* cell strain was used to determine the bacterial inhibitory capacity. *E. coli* colonies grown in solutions containing different amounts of LDH nanomaterial were obtained. After the membranes were exposed to *E. coli* solutions for 24 h they were removed and submerged in sterilized water. Then, *E. coli* colonies in suspension were obtained. The images of bacterial colonies were used to determine the antibacterial characteristics. The detailed procedure was described in a previous study [24].

3. Results and Discussion

3.1. Characterization of ZnFeCe LDH

SEM image shows regularly distributed particles with flake-like shapes, which is the characteristic appearance of the LDHs (Figure 1a,b) [25]. TEM images show LDH plates with interplanar spacings of about 0.32 and 0.29 nm of lattice planes (1 1 0) and (0 0 9) (Figure 1c,d). The XRD spectrum of the ZnFeCe LDH (Figure 1e) exhibits reflection peaks located at 10.01°, 23.62°, 28.28°, 32.87°, 34.73°, 39.15°, 49.26°, 58.56°, 62.42° which are indexed to 003, 006, 110, 009, 012, 015, 018, 110, 113 crystalline planes [24,26]. The mean crystallite size of the ZnFeCe LDH was determined as 21.3 nm using the Debye-Scherrer formula [27]. The BET surface, total pore volume, and average pore size of the ZnFeCe LDH were found as 43.88 m²/g, 0.106 cm³/g, and 9.7 nm, respectively.

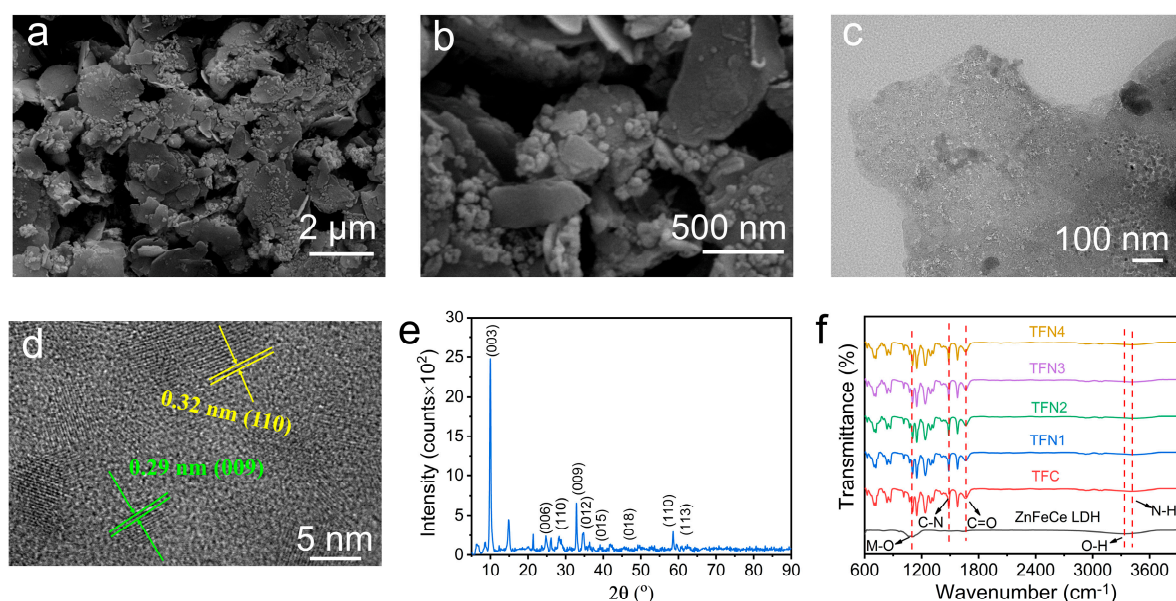


Figure 1. Scanning electron microscope (SEM) images (a,b) and high-resolution transmission electron microscopy HRTEM images (c,d) of the ZnFeCe LDH; X-ray powder diffraction (XRD) spectrum of ZnFeCe LDH (e); Fourier-transform infrared (FTIR) analysis of ZnFeCe LDH, TFC, and TFN membranes (f).

3.2. Characterization of TFC and TFN Membranes

Functional groups of the fabricated membranes were examined using FTIR analysis (Figure 1f). Strong band at 1630 cm^{-1} is due to the C=O stretching of the amide group, which confirms that the top of the membranes was successfully covered by the PA layer [28]. The peak observed at 1456 cm^{-1} can be attributed to the C-N band of the amide group. Additionally, the band at 3400 cm^{-1} was attributed to the occurrence of -COOH groups that are produced by partial hydrolysis of TMC [29]. In the FTIR spectrum of ZnFeCe LDH, the stretching vibration between the hydroxyl groups of the interlayer water and the hydroxide layers caused a large peak at around 3459 cm^{-1} [24]. The peak around 1638 cm^{-1} can be attributed to the bending vibration of interlayer water molecules. The bands around 1092 cm^{-1} and 808 cm^{-1} were due to the vibration of M-O-H and O-M-O bonds in the LDH brucite-like layers [30]. The hydrophilicity of the membrane surface increases due to the abundance of hydroxyl groups on the surface of LDH. However, the peaks related to the LDH nanomaterial were not strongly observed in FTIR spectra because low LDH concentration was added into the PA layer during the IP process. Furthermore, it was previously reported that the LDH peaks may overlap with peaks corresponding to functional groups for example imide, amide, and hydroxyls [31,32].

SEM/EDS analyses of the TFC and TFN 3 membranes are shown in Figure 2. The presence of Ce, Fe, and Zn elements in the EDS analysis shows that LDH nanoparticles were successfully added to the top layer of the membrane. The AFM images and the roughness parameters (Ra, Rz, and Rrms) of TFC and TFN 3 are presented in Figure 3. Addition of LDH resulted in a smoother surface, which was indicated by lower Ra of TFN 3 (1.819 nm) than that of TFC (3.854 nm). The reduction in surface roughness was linked to the fabrication of smaller nodules on the membrane surface during the IP process. A smooth membrane surface with fewer valley and ridge structures provides enhanced antifouling characteristics [33].

According to the cross-sectional images of the fabricated membranes (TFC and TFN 3), a thin film layer appeared on the top of the PES substrate (Figure 2a). The selective layer thicknesses of the TFC and TFN 3 membranes were determined as 104 and 75 nm, respectively. The reduction in selective layer thickness causes the membrane to be less

resistant to the transport of water molecules and further increases the permeability of the fabricated membrane.

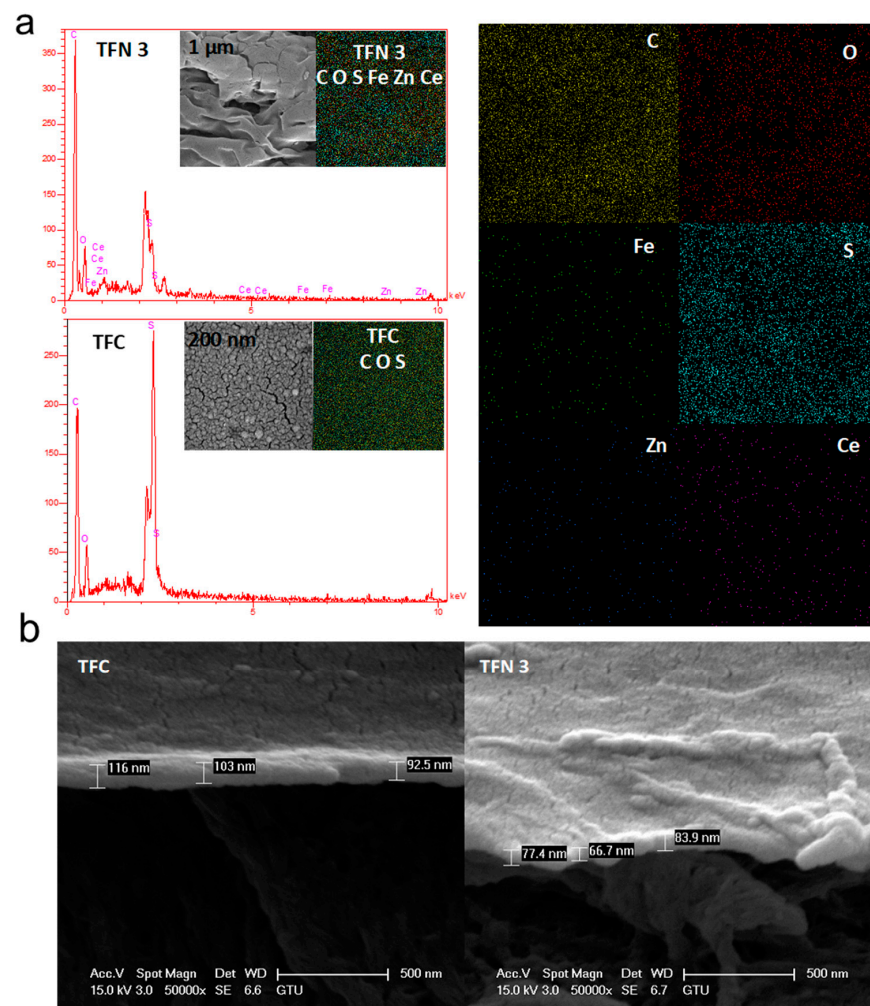


Figure 2. EDS mapping (a) and cross-section images (b) of TFC and TFN 3 membranes.

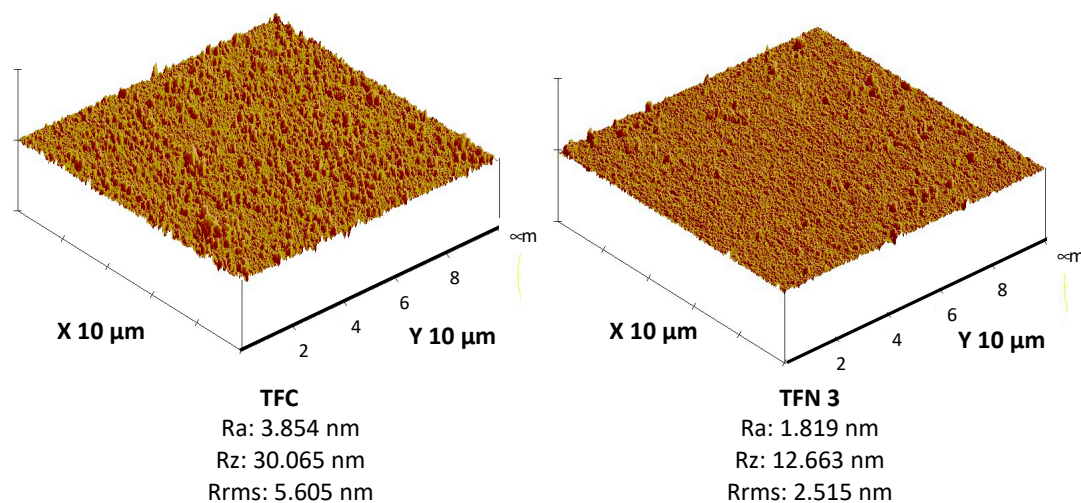


Figure 3. AFM analysis of TFC and TFN 3 membranes.

Figure 4a shows the contact angle and pure water flux measurements of the fabricated membranes. Raw TFC membrane had the highest water contact angle (67.7°) due to its

low hydrophilic surface. Among TFN membranes, TFN 3 with an LDH loading of 0.1% wt. experienced the lowest contact angle (39.2°). The improvement in membrane hydrophilicity was primarily attributed to the hydrophilic groups of LDH [34]. More water molecules can be attracted to the hydrophilic membrane surfaces, which is beneficial for water permeance. Additionally, increasing the hydrophilicity of the membrane surface can lead to higher fouling resistance, which mitigates the possible accumulation of hydrophobic foulants on the membrane surface [35].

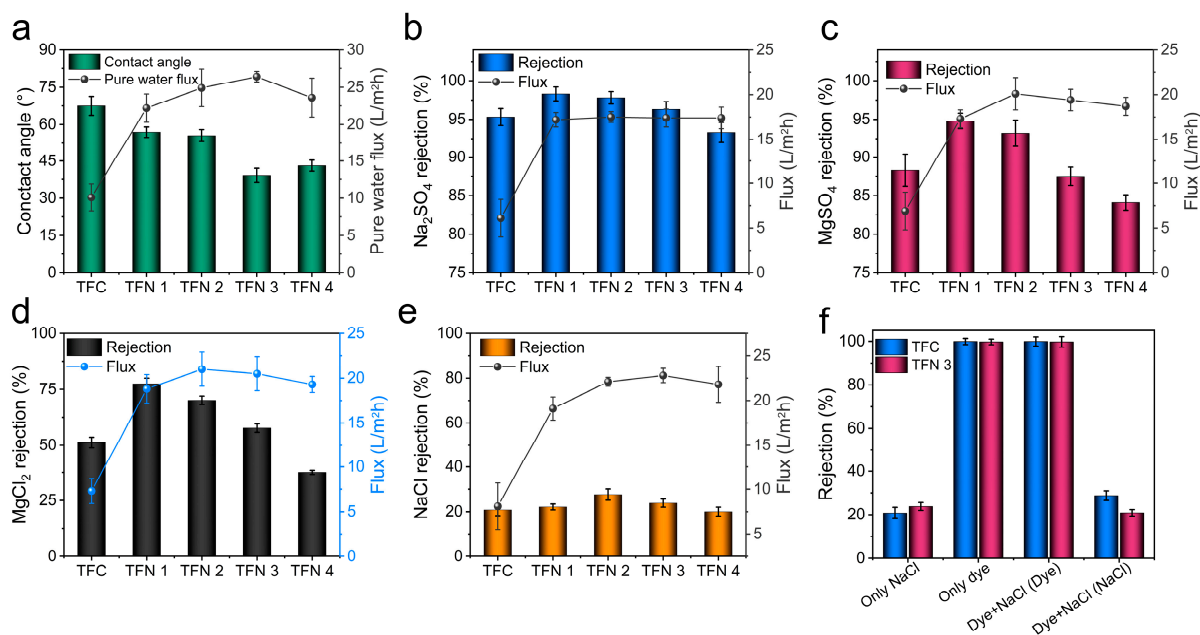


Figure 4. Water contact angle and pure water flux measurements of the fabricated membrane (a); Flux and rejection of the fabricated membranes for different salts, Na₂SO₄ (b), MgSO₄ (c), MgCl₂ (d), and NaCl (e); Dye/salt separation performances of TFC and TFN 3 membranes (f).

The pure water fluxes were measured to evaluate the water permeance of fabricated membranes (Table S1 in the Supplementary materials). As shown in Figure 4a, pristine TFC had the lowest pure water flux ($10.1 \text{ L m}^{-2} \text{ h}^{-1}$) which is attributed to its smooth and dense structure. Similar to the water contact angle measurements, greater LDH loading caused an increase in the pure water fluxes in TFN membranes. TFN 3 membrane achieved the highest water flux with $26.4 \text{ L m}^{-2} \text{ h}^{-1}$, which corresponds to a 161% flux increment compared to the TFC membrane. Greater water flux values of TFN membranes can be related to the formation of interlayer pathways of LDH that facilitate water transport through the membrane [36]. Additionally, increased membrane hydrophilicity caused by the presence of LDHs also contributed to the greater water flux performance of TFN membranes. However, the decrease in both the membrane contact angle and pure water flux measurements when the LDH content exceeded 0.1% wt. could be caused by agglomerated particles that block water pathways for transport [37].

3.3. Desalination Performance

The desalination performances of the TFC and TFN membranes was determined by evaluating the rejection of Na₂SO₄, MgSO₄, NaCl, and MgCl₂ solutions at a pressure of 10 bar (Figure 4b–e). TFN 1 membrane achieved the highest salt rejection performances towards Na₂SO₄ (98.3%), MgSO₄ (88.3%), MgCl₂ (77.4%), and NaCl (22.1%). All membranes exhibit an excellent rejection performance (with a rejection higher than 95% and 88% for Na₂SO₄ and MgSO₄, respectively) for divalent ions (Table S2 in the Supplementary materials). The salt rejection performance order was observed as NaCl < MgCl₂ < MgSO₄ < Na₂SO₄ for all of the fabricated membranes. Nanofiltration (NF) separation mechanisms are mainly gov-

erned by Donnan effects and membrane pore diameter [38,39]. As a result, the membranes with negative surface charges had higher rejection values for divalent anions than low-valent anions because of the higher electrostatic repulsion of high-valent anions [40]. The mechanism of NF is also influenced by the diffusion coefficient, ion radius, and hydrated radius of each salt. Its more challenging for ions with low diffusion coefficients, such as SO_4^{2-} , to pass through the membrane, resulting in higher rejection of SO_4^{2-} ions [40,41]. A t-test analysis was performed on two membranes (TFC and TFN 3) in terms of the effect of LDH addition on salt rejection and water permeability. According to the t-test results (Table S3 in the Supplementary Materials), the fluxes of TFC and TFN 3 membranes were statistically different ($p < 0.05$), which implied that the LDH addition on the membrane surface has a significant effect on water permeance. On the other hand, the p values for salt rejections, which were generally higher than 0.05, indicated that LDH addition on the membrane surface has an insignificant effect on membrane salt rejection performance.

3.4. Dye and Salt Separation Performance

The dye removal performances of the TFC and TFN 3 membranes were investigated by filtrating different dye/salt solutions. Dye removal was carried out with two different solutions: A 100 mg/L dye solution or a 100 mg/L dye solution containing 1 g/L NaCl (Figure 4f). Both of the membranes achieved higher than 99% dye removal efficiencies regardless of the presence of NaCl. While the TFF 3 membrane only removed 99.7% of the dye solution, it achieved 20.9% removal efficiency for only 1 g/L NaCl solution. Notably, TFN 3 membrane performed slightly better at filtrating only NaCl solution and dye + NaCl mixture compared with the TFC membrane. It was attributed to residual dye on the membrane surface resulting in decreasing penetration of salts [42].

3.5. Self-Cleaning Properties

The self-cleaning properties of TFC and TFN 3 membranes were evaluated after filtrating a dye solution. For this purpose, membranes were operated with a 1000 mg/L dye solution until a decrease in the flux was observed due to the coverage of the membrane surfaces with dye molecules. The images of TFC and TFN membranes after 15 min photocatalytic degradation under visible light were illustrated in Figure 5. TFN 3 membrane demonstrated low fouling and high self-cleaning ability due to the presence of ZnFeCe LDH in the membrane surface, while the TFC membrane had limited self-cleaning ability under visible light [43].

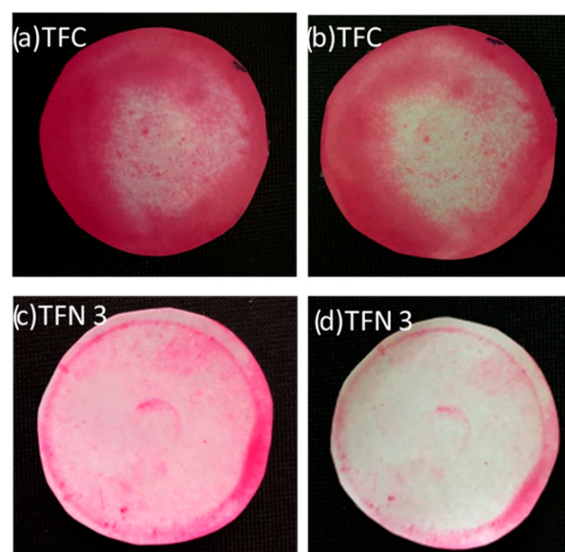


Figure 5. Photographs of the TFC membrane before (a) and after photocatalytic treatment (b); Photographs of the TFN membrane before (c) and after (d) photocatalytic treatment.

3.6. Antibacterial Properties

Antibacterial properties of TFC and TFN 3 membrane were determined by bacterial viability inhibition test. Cell viability of ZnFeCe LDH against *E. coli* cell strain was used to determine the bacterial inhibition capacity. *E. coli* colonies grown in solutions containing different amounts of LDH were obtained and the images of bacterial colonies were presented in Figure 6a–c. The disks containing LDH showed great inhibition properties compared with the control disk without LDH. An increase in LDH content resulted in higher bacterial inhibition capacity, which is consistent with earlier studies [24]. Additionally, Figure 6d,e shows the *E. coli* colonies in suspension after TFC and TFN 3 membranes were exposed to *E. coli*. The lower number of rod-like structures in the TFN 3 membrane sample than that of TFC proved the inhibition of *E. coli* due to the presence of LDH. The results exhibited that LDH nanomaterial imparts antibacterial properties to the membrane.

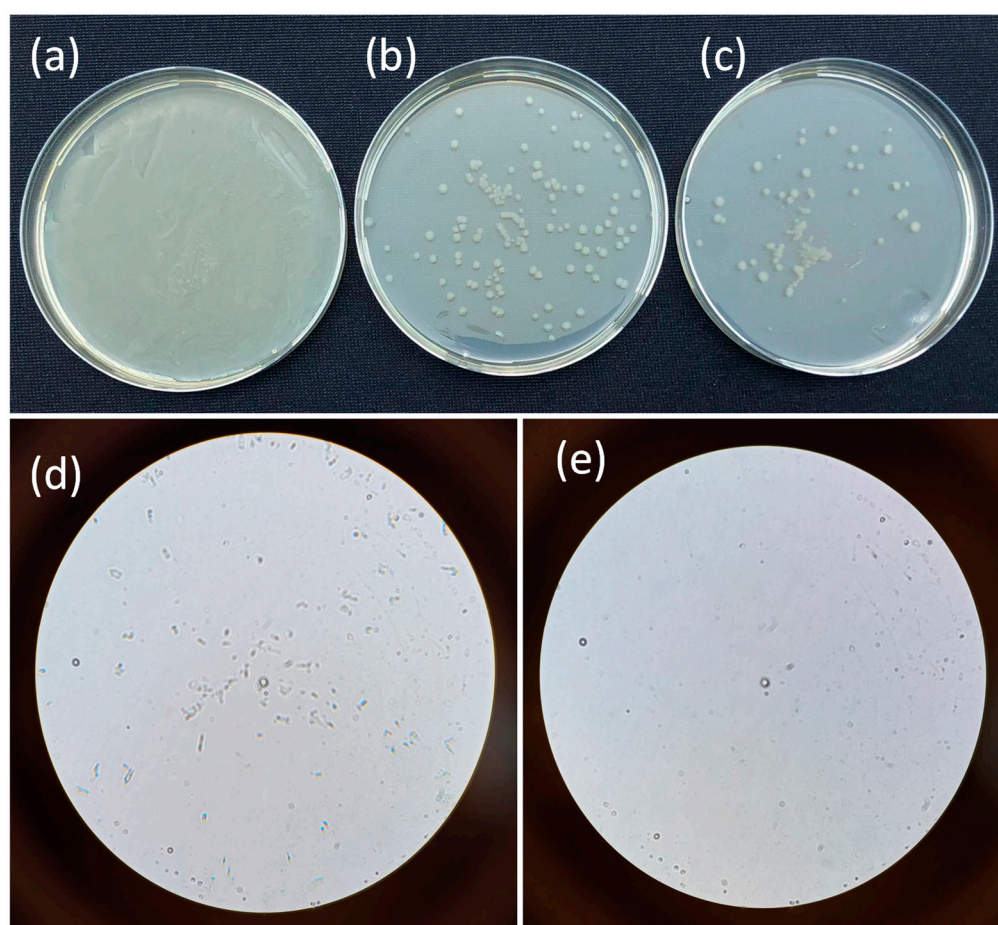


Figure 6. Plate samples of formed *E. coli* cells (a) without the addition of LDH (b) *E. coli* + DMAC + 250 mg/L LDH, and (c) *E. coli* + DMAC + 500 mg/L LDH, *E. coli* colonies grown on TFC (d) and TFN 3 membranes (e).

4. Conclusions

This study presented the incorporation of ZnFeCe LDH into the TFC membrane using the IP technique. PA layer was successfully formed on the top of the membrane surfaces according to FTIR. The presence of Ce, Fe, and Zn elements on the membrane surface was confirmed by EDS mapping of the TFN membrane. The addition of ZnFeCe LDH into the PA layer resulted in a smoother surface that contributed to enhanced antifouling properties. Among TFN membranes containing different LDH loadings, the membrane with 0.1% wt LDH (TFN 3) showed a decrease in the water contact angle of the TFC membrane from 67.7° to 39.2°. Owing to its enhanced hydrophilicity, TFN 3 membrane achieved 161%

higher pure water flux than that of the TFC membrane. All membranes showed great rejection performances (with a rejection higher than 95% and 88% for Na_2SO_4 and MgSO_4 , respectively) for divalent ions. During the photocatalytic tests, TFN 3 membrane demonstrated low fouling and high self-cleaning ability. In contrast, TFC membrane had limited self-cleaning ability under visible light. Additionally, *E. coli* inhibition tests showed that ZnFeCe LDH imparted antibacterial properties to the TFN 3 membrane.

Supplementary Materials: The following supporting information can be downloaded at: <https://www.mdpi.com/article/10.3390/w15020264/s1>, Table S1: Water permeance of fabricated membranes; Table S2: Rejection values of the fabricated membrane; and Table S3: *t*-test results for comparing TFC and TFN 3 membrane.

Author Contributions: Supervision, C.B. and A.K.; writing—original draft preparation, C.B. and B.O.-U.; experiments, C.B., B.O.-U., B.S., E.B.A., B.C.-G. and R.K.; formal analysis, B.S., E.B.A. and B.C.-G.; funding acquisition, C.B. and A.K.; reviewing and editing, R.K. and A.K. All authors have read and agreed to the published version of the manuscript.

Funding: This research was funded by the Scientific and Technical Research Council of Turkey (TUBITAK, Projects numbers: 120Y350 and 2209 A).

Data Availability Statement: Data sharing not applicable.

Acknowledgments: We would like to thank the Scientific and Technical Research Council of Turkey (TUBITAK, Projects Numbers: 120Y350 and 2209 A) for funding the research project.

Conflicts of Interest: The authors declare no conflict of interest.

References

1. Tzanakakis, V.A.; Paranychanakis, N.V.; Angelakis, A.N. Water Supply and Water Scarcity. *Water* **2020**, *12*, 2347. [CrossRef]
2. Vatanpour, V.; Faghani, S.; Keyikoglu, R.; Khataee, A. Enhancing the permeability and antifouling properties of cellulose acetate ultrafiltration membrane by incorporation of ZnO@graphitic carbon nitride nanocomposite. *Carbohydr. Polym.* **2021**, *256*, 117413. [CrossRef] [PubMed]
3. Ji, C.; Zhai, Z.; Jiang, C.; Hu, P.; Zhao, S.; Xue, S.; Yang, Z.; He, T.; Niu, Q.J. Recent advances in high-performance TFC membranes: A review of the functional interlayers. *Desalination* **2021**, *500*, 114869. [CrossRef]
4. Wei, X.; Liu, Y.; Zheng, J.; Wang, X.; Xia, S.; Van der Bruggen, B. A critical review on thin-film nanocomposite membranes enabled by nanomaterials incorporated in different positions and with diverse dimensions: Performance comparison and mechanisms. *J. Membr. Sci.* **2022**, *661*, 120952. [CrossRef]
5. Johnson, D.J.; Hilal, N. Nanocomposite nanofiltration membranes: State of play and recent advances. *Desalination* **2022**, *524*, 115480. [CrossRef]
6. Zhao, D.L.; Japip, S.; Zhang, Y.; Weber, M.; Maletzko, C.; Chung, T.-S. Emerging thin-film nanocomposite (TFN) membranes for reverse osmosis: A review. *Water Res.* **2020**, *173*, 115557. [CrossRef] [PubMed]
7. Jeong, B.-H.; Hoek, E.M.; Yan, Y.; Subramani, A.; Huang, X.; Hurwitz, G.; Ghosh, A.K.; Jawor, A. Interfacial polymerization of thin film nanocomposites: A new concept for reverse osmosis membranes. *J. Membr. Sci.* **2007**, *294*, 1–7. [CrossRef]
8. Fetanat, M.; Keshtiar, M.; Keyikoglu, R.; Khataee, A.; Daiyan, R.; Razmjou, A. Machine learning for design of thin-film nanocomposite membranes. *Sep. Purif. Technol.* **2021**, *270*, 118383. [CrossRef]
9. Güvensoy-Morkoyun, A.; Kürklü-Kocaoğlu, S.; Yıldırım, C.; Velioglu, S.; Karahan, H.E.; Bae, T.-H.; Tantekin-Ersolmaz, B. Carbon nanotubes integrated into polyamide membranes by support pre-infiltration improve the desalination performance. *Carbon N. Y.* **2021**, *185*, 546–557. [CrossRef]
10. Wu, T.; Prasetya, N.; Li, K. Recent advances in aluminium-based metal-organic frameworks (MOF) and its membrane applications. *J. Membr. Sci.* **2020**, *615*, 118493. [CrossRef]
11. Du, Y.; Huang, L.; Wang, Y.; Yang, K.; Tang, J.; Wang, Y.; Cheng, M.; Zhang, Y.; Kipper, M.J.; Belfiore, L.A.; et al. Recent developments in graphene-based polymer composite membranes: Preparation, mass transfer mechanism, and applications. *J. Appl. Polym. Sci.* **2019**, *136*, 47761. [CrossRef]
12. Kumar, R.; Basak, B.; Jeon, B.-H. Sustainable production and purification of succinic acid: A review of membrane-integrated green approach. *J. Clean. Prod.* **2020**, *277*, 123954. [CrossRef]
13. Rodrigues, R.; Mierzwa, J.C.; Vecitis, C.D. Mixed matrix polysulfone/clay nanoparticles ultrafiltration membranes for water treatment. *J. Water Process. Eng.* **2019**, *31*, 100788. [CrossRef]
14. Shaiju, P.; Dorian, B.-B.; Senthamaraiannan, R.; Padamati, R.B. Biodegradation of poly (butylene succinate)(PBS)/stearate modified magnesium-aluminium layered double hydroxide composites under marine conditions prepared via melt compounding. *Molecules* **2020**, *25*, 5766. [CrossRef]

15. Chaillot, D.; Bennici, S.; Brendlé, J. Layered double hydroxides and LDH-derived materials in chosen environmental applications: A review. *Environ. Sci. Pollut. Res.* **2020**, *28*, 24375–24405. [[CrossRef](#)] [[PubMed](#)]
16. Jia, Z.; Hao, S.; Lu, X. Exfoliated Mg–Al–Fe layered double hydroxides/polyether sulfone mixed matrix membranes for adsorption of phosphate and fluoride from aqueous solutions. *J. Environ. Sci.* **2018**, *70*, 63–73. [[CrossRef](#)] [[PubMed](#)]
17. Zhao, S.; Zhu, H.; Wang, Z.; Song, P.; Ban, M.; Song, X. A loose hybrid nanofiltration membrane fabricated via chelating-assisted in-situ growth of Co/Ni LDHs for dye wastewater treatment. *Chem. Eng. J.* **2018**, *353*, 460–471. [[CrossRef](#)]
18. Mutharasi, Y.; Zhang, Y.; Weber, M.; Maletzko, C.; Chung, T.-S. Novel reverse osmosis membranes incorporated with Co-Al layered double hydroxide (LDH) with enhanced performance for brackish water desalination. *Desalination* **2021**, *498*, 114740. [[CrossRef](#)]
19. Azad, H.; Mohsennia, M. A novel free-standing polyvinyl butyral-polyacrylonitrile/ZnAl-layered double hydroxide nanocomposite membrane for enhanced heavy metal removal from wastewater. *J. Membr. Sci.* **2020**, *615*, 118487. [[CrossRef](#)]
20. Qi, M.; Li, W.; Zheng, X.; Li, X.; Sun, Y.; Wang, Y.; Li, C.; Wang, L. Cerium and Its Oxidant-Based Nanomaterials for Antibacterial Applications: A State-of-the-Art Review. *Front. Mater.* **2020**, *7*, 213. [[CrossRef](#)]
21. Chang, C.-J.; Lin, C.-Y.; Hsu, M.-H. Enhanced photocatalytic activity of Ce-doped ZnO nanorods under UV and visible light. *J. Taiwan Inst. Chem. Eng.* **2014**, *45*, 1954–1963. [[CrossRef](#)]
22. Suárez-Quezada, M.; Romero-Ortiz, G.; Suárez, V.; Morales-Mendoza, G.; Lartundo-Rojas, L.; Navarro-Cerón, E.; Tzompantzi, F.; Robles, S.; Gómez, R.; Mantilla, A. Photodegradation of phenol using reconstructed Ce doped Zn/Al layered double hydroxides as photocatalysts. *Catal. Today* **2016**, *271*, 213–219. [[CrossRef](#)]
23. Keyikoğlu, R.; Doğan, I.N.; Khataee, A.; Orooji, Y.; Kobya, M.; Yoon, Y. Synthesis of visible light responsive ZnCoFe layered double hydroxide towards enhanced photocatalytic activity in water treatment. *Chemosphere* **2022**, *309*, 136534. [[CrossRef](#)] [[PubMed](#)]
24. Balcik, C.; Ozbey-Unal, B.; Cifcioglu-Gozuacik, B.; Keyikoglu, R.; Karagunduz, A.; Khataee, A. Fabrication of PSf nanocomposite membranes incorporated with ZnFe layered double hydroxide for separation and antifouling aspects. *Sep. Purif. Technol.* **2022**, *285*, 120354. [[CrossRef](#)]
25. Xie, Z.-H.; Zhou, H.-Y.; He, C.-S.; Pan, Z.-C.; Yao, G.; Lai, B. Synthesis, application and catalytic performance of layered double hydroxide based catalysts in advanced oxidation processes for wastewater decontamination: A review. *Chem. Eng. J.* **2021**, *414*, 128713. [[CrossRef](#)]
26. Zhang, Y.; Jing, S.; Liu, H. Reactivity and mechanism of bromate reduction from aqueous solution using Zn–Fe(II)–Al layered double hydroxides. *Chem. Eng. J.* **2015**, *266*, 21–27. [[CrossRef](#)]
27. Thakar, M.A.; Jha, S.S.; Phasinam, K.; Manne, R.; Qureshi, Y.; Babu, V.H. X ray diffraction (XRD) analysis and evaluation of antioxidant activity of copper oxide nanoparticles synthesized from leaf extract of *Cissus vitiginea*. *Mater. Today Proc.* **2022**, *51*, 319–324. [[CrossRef](#)]
28. Misdan, N.; Lau, W.; Ismail, A.; Matsuura, T. Formation of thin film composite nanofiltration membrane: Effect of polysulfone substrate characteristics. *Desalination* **2013**, *329*, 9–18. [[CrossRef](#)]
29. Li, H.; Shi, W.; Zhang, Y.; Du, Q.; Qin, X.; Su, Y. Improved performance of poly(piperazine amide) composite nanofiltration membranes by adding aluminum hydroxide nanospheres. *Sep. Purif. Technol.* **2016**, *166*, 240–251. [[CrossRef](#)]
30. Bharali, D.; Deka, R.C. Preferential adsorption of various anionic and cationic dyes from aqueous solution over ternary Cu Mg Al layered double hydroxide. *Colloids Surfaces A Physicochem. Eng. Asp.* **2017**, *525*, 64–76. [[CrossRef](#)]
31. Li, C.; Li, S.; Tian, L.; Zhang, J.; Su, B.; Hu, M.Z. Covalent organic frameworks (COFs)-incorporated thin film nanocomposite (TFN) membranes for high-flux organic solvent nanofiltration (OSN). *J. Membr. Sci.* **2019**, *572*, 520–531. [[CrossRef](#)]
32. Yao, Z.; Guo, H.; Yang, Z.; Qing, W.; Tang, C.Y. Preparation of nanocavity-contained thin film composite nanofiltration membranes with enhanced permeability and divalent to monovalent ion selectivity. *Desalination* **2018**, *445*, 115–122. [[CrossRef](#)]
33. Abdullah, N.; Gohari, R.; Yusof, N.; Ismail, A.; Juhana, J.; Lau, W.; Matsuura, T. Polysulfone/hydrous ferric oxide ultrafiltration mixed matrix membrane: Preparation, characterization and its adsorptive removal of lead (II) from aqueous solution. *Chem. Eng. J.* **2015**, *289*, 28–37. [[CrossRef](#)]
34. Meng, Z.; Zhang, Y.; Zhang, Q.; Chen, X.; Liu, L.; Komarneni, S.; Lv, F. Novel synthesis of layered double hydroxides (LDHs) from zinc hydroxide. *Appl. Surf. Sci.* **2017**, *396*, 799–803. [[CrossRef](#)]
35. Bano, S.; Mahmood, A.; Kim, S.-J.; Lee, K.-H. Graphene oxide modified polyamide nanofiltration membrane with improved flux and antifouling properties. *J. Mater. Chem. A Mater.* **2015**, *3*, 2065–2071. [[CrossRef](#)]
36. Tajuddin, M.H.; Yusof, N.; Abdullah, N.; Abidin, M.N.Z.; Salleh, W.N.W.; Ismail, A.F.; Matsuura, T.; Hairom, N.H.H.; Misdan, N. Incorporation of layered double hydroxide nanofillers in polyamide nanofiltration membrane for high performance of salts rejections. *J. Taiwan Inst. Chem. Eng.* **2019**, *97*, 1–11. [[CrossRef](#)]
37. Dong, H.; Wu, L.; Zhang, L.; Chen, H.; Gao, C. Clay nanosheets as charged filler materials for high-performance and fouling-resistant thin film nanocomposite membranes. *J. Membr. Sci.* **2015**, *494*, 92–103. [[CrossRef](#)]
38. Rezaia, J.; Vatanpour, V.; Shockravi, A.; Ehsani, M. Preparation of novel carboxylated thin-film composite polyamide-polyester nanofiltration membranes with enhanced antifouling property and water flux. *React. Funct. Polym.* **2018**, *131*, 123–133. [[CrossRef](#)]
39. Zeng, Y.; Wang, L.; Zhang, L.; Yu, J.Q. An acid resistant nanofiltration membrane prepared from a precursor of poly(s-triazine-amine) by interfacial polymerization. *J. Membr. Sci.* **2018**, *546*, 225–233. [[CrossRef](#)]

40. Xie, Q.; Shao, W.; Zhang, S.; Hong, Z.; Wang, Q.; Zeng, B. Enhancing the performance of thin-film nanocomposite nanofiltration membranes using MAH-modified GO nanosheets. *RSC Adv.* **2017**, *7*, 54898–54910. [[CrossRef](#)]
41. Li, X.; Zhao, C.; Yang, M.; Yang, B.; Hou, D.; Wang, T. Reduced graphene oxide-NH₂ modified low pressure nanofiltration composite hollow fiber membranes with improved water flux and antifouling capabilities. *Appl. Surf. Sci.* **2017**, *419*, 418–428. [[CrossRef](#)]
42. Xu, M.; Feng, X.; Liu, Z.; Han, X.; Zhu, J.; Wang, J.; Van der Bruggen, B.; Zhang, Y. MOF laminates functionalized polyamide self-cleaning membrane for advanced loose nanofiltration. *Sep. Purif. Technol.* **2021**, *275*, 119150. [[CrossRef](#)]
43. Zong, Y.; Ma, S.; Xue, J.; Gu, J.; Wang, M. Bifunctional NiAlFe LDH-coated membrane for oil-in-water emulsion separation and photocatalytic degradation of antibiotic. *Sci. Total Environ.* **2021**, *751*, 141660. [[CrossRef](#)] [[PubMed](#)]

Disclaimer/Publisher's Note: The statements, opinions and data contained in all publications are solely those of the individual author(s) and contributor(s) and not of MDPI and/or the editor(s). MDPI and/or the editor(s) disclaim responsibility for any injury to people or property resulting from any ideas, methods, instructions or products referred to in the content.